Biophysical Journal Volume 92 March 2007 1573–1584

Three-Dimensional Dynamic Structure of the Liquid-Ordered Domain in Lipid Membranes as Examined by Pulse-EPR Oxygen Probing

Witold K. Subczynski,* Anna Wisniewska,*† James S. Hyde,* and Akihiro Kusumi‡
*Department of Biophysics, Medical College of Wisconsin, Milwaukee, Wisconsin 53226; †Department of Biophysics, Faculty of Biochemistry, Biophysics and Biotechnology, Jagiellonian University, Krakow, Poland; ‡Membrane Mechanisms Project, ICORP, Japan Science and Technology Agency, The Institute for Frontier Medical Sciences, Kyoto University, Shougoin, Kyoto 606-8507, Japan

ABSTRACT Membranes made of dimyristoylphosphatidylcholine and cholesterol, one of the simplest paradigms for the study of liquid ordered-disordered phase separation, were investigated using a pulse-EPR spin-labeling method in which bimolecular collision of molecular oxygen with the nitroxide spin label is measured. This method allowed discrimination of liquid-ordered, liquid-disordered, and solid-ordered domains because the collision rates (OTP) differ in these domains. Furthermore, the oxygen transport parameter (OTP) profile across the bilayer provides unique information about the three-dimensional dynamic organization of the membrane domains. First, the OTP in the bilayer center in the liquid-ordered domain was comparable to that in the liquid-disordered domain without cholesterol, but the OTP near the membrane surface (up to carbon 9) was substantially smaller in the ordered domain, i.e., the cholesterol-based liquid-ordered domain is ordered only near the membrane surface, still retaining high levels of disorder in the bilayer center. This property may facilitate lateral mobility in ordered domains. Second, in the liquid-disordered domain, the domains with ~5 mol % cholesterol exhibited higher OTP than those without cholesterol, everywhere across the membrane. Third, the transmembrane OTP profile in the liquid-ordered domain that contained 50 mol % cholesterol dramatically differed from that which contained 27 mol % cholesterol.

INTRODUCTION

Recently, extensive attention has been paid to the cholesterol-dependent liquid-ordered phase in the membrane because of the enhanced interest in membrane microdomains, particularly so-called raft domains or rafts. The interest in rafts spans almost all areas of biomedical research related to cell-cell signaling and trafficking of lipids and proteins in cells (see recent reviews (1–8)). Although the clear definition for raft domains in various membranes of cells, particularly for those before extracellular or intracellular stimulation, has to wait for further advancement of raft-related research, it appears that raft researchers could gain some insight into the structure of, and the molecular interactions in, raft domains by understanding liquid-ordered domains and liquid-liquid phase separations in binary or ternary mixtures of lipids including cholesterol and saturated-chain lipids. Simons and Vaz (9) extensively furthered this concept, insisting that, after weighting all the existing observations, ''rafts could be considered domains of a liquid-ordered phase.'' This statement has not been tested because of the lack of experimental methods that can be applied to the raft domains in live cells (10,11), but what we have learned regarding the molecular components and interactions that lead to the formation of the liquid-ordered phase in artificial membranes is likely to make great contributions for understanding the formation mechanism, structure, lifetime, and dynamics of raft domains in the membranes of cells (3,6–8,12–14).

Based on this concept, we believe that the efforts to extensively characterize the liquid-ordered domains are important (see Almeida et al. (15) for terminological discussion regarding ''phases'' and ''domains''). In fact, our understanding of the molecular dynamics within and into/out of liquid-ordered domains (16–18), their structures and mechanics (4,9,19–21), and the dynamics of the whole liquid-ordered domains is making progress (6,22–24). However, one of the missing issues in the research in this field is the understanding of the molecular dynamics and structures in the third dimension, namely, in the direction of the depth in the membrane. Because the membrane, and thus the liquid-ordered domain, is not really a two-dimensional structure, knowledge of the molecular events in the depth dimension is important.

In this research, we characterized three-dimensional dynamic structures of liquid-ordered domains. This achievement became possible by use of a very small probe, i.e., molecular oxygen. In this approach, a variety of lipid spin probes were incorporated in the membrane for probing at specific depths and specific domains (Fig. 1), and the rate of collision between molecular oxygen and the nitroxide moiety attached to a specific location in the lipid was measured using the pulse EPR method. Previously, we

Submitted September 14, 2006, and accepted for publication November 2, 2006.

Address reprint requests to Witold K. Subczynski, Dept. of Biophysics, Medical College of Wisconsin, 8701 Watertown Plank Road, Milwaukee, WI 53226. Tel.: 414-456-4038; Fax: 414-456-6512; E-mail: subczyn@mcw.edu.

Abbreviations: *n*-SASL, *n*-doxylstearic acid spin labels (where $n = 7$ or 9); DOT, discrimination by oxygen transport; DMPC, L-α-dimyristoylphosphatidylcholine; OTP, oxygen transport parameter; T-PC, tempocholine-1-palmitoyl-2-oleoylphosphatidic acid ester; *n*-PC, 1-palmitoyl-2-(*n*-doxylstearoyl)phosphatidylcholine (where $n = 5$, 7, 10, 12, 14, or 16); FOT, fast oxygen transport; SLOT, slow oxygen transport; l_o, liquid-ordered; l_d, liquid-disordered; s_o, solid ordered.

0006-3495/07/03/1573/12 $2.00
doi: 10.1529/biophysj.106.097568

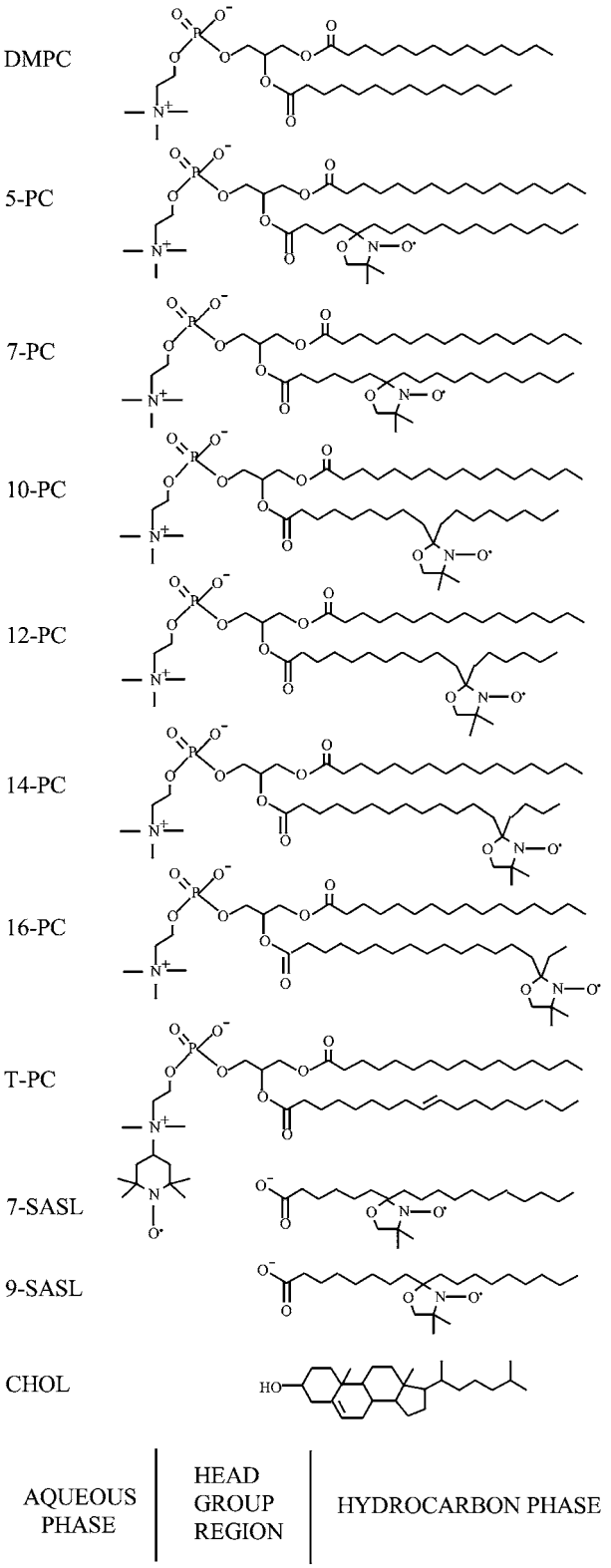

FIGURE 1 Chemical structures of phospholipid-type spin labels, including *n*-PCs, T-PC, and *n*-SASLs. Chemical structures of DMPC and cholesterol are included to illustrate approximate locations of nitroxide moieties across the membrane. In the fluid phase, alkyl chains tend to have many *gauche* conformations, and chain length projected to the membrane normal would be shorter than that depicted here.

reported the existence of vertical fluctuations of the nitroxide moiety of stearic acid spin labels toward the polar surface of the lipid bilayers (25–27). Measurements were made of bimolecular collision rates between nitroxide moieties at different locations on the alkyl chain. From these studies it can be presumed that distributions of the vertical positions of the nitroxide moiety on *n*-SASL and *n*-PC in the membrane exist, with the mean value of each distribution shifting toward the center as the quantum *n* increases. Positions of carbon atoms in the alkyl chain have been determined by neutron diffraction (28), which showed that the mean positions of these carbons (or free radical moieties attached to those carbons) can be defined with accuracy ± 1 Å, even in the liquid-crystalline state. Assuming a Gaussian distribution of the labeled segments in the projection on the bilayer normal, these authors report that the time-averaged positional fluctuations increase from 1.5 Å for the C-4 position to 3.4 Å for the C-12 position. It can be concluded that a nitroxide moiety stays at the position determined by neutron diffraction for most of the time.

Our previous studies indicated that the oxygen collision rate, which is a product of local concentration and local diffusion coefficient of molecular oxygen within the membrane, is a very sensitive measure of the presence and the movement of free volume, which may be very small—just sufficient to contain a single molecule of oxygen in the membrane. The small size and appropriate level of hydrophobicity of molecular oxygen allow it to enter the small vacant pockets that are transiently formed in the lipid bilayer membrane. Therefore, collision rates between molecular oxygen and nitroxide spin labels at specific locations in the membrane are sensitive to the dynamics of *gauche-trans* isomerization of lipid hydrocarbon chains and to the structural nonconformability of neighboring lipids (29–32). For example, incorporation of cholesterol into bilayers made of saturated and unsaturated phosphatidylcholines greatly reduces the oxygen collision rate at the place where cholesterol's rigid steroid ring structure is located but increases it in the central part of the membrane where the bulky cyclic backbone of cholesterol cannot reach (31,33). Such observations were made possible by using the very small (and hydrophobic) probe of molecular oxygen in these measurements. Additionally, oxygen collision rates or the oxygen transport parameter (OTP) could be obtained in coexisting domains without the need for their separation (34–37). We employed this approach in the present investigation. The profiles of oxygen collision rates across the membrane were obtained, which provide useful information on the three-dimensional dynamic structure of the liquid-ordered domain (31,33–35,38–41).

As the paradigm for the present study, we employed one of the simplest model membranes that contains the liquid-ordered phase: a binary mixture of L-α-dimyristoylphosphatidylcholine and cholesterol. The phase diagram and lipid motion have been well characterized (15,42–45). The phase

diagram based on Almeida et al. (45) is schematically shown in Fig. 2 and is used as a guideline for the presentation of our data.

MATERIALS AND METHODS

Materials

DMPC, cholesterol, and phospholipid spin labels were obtained from Avanti Polar Lipids (Alabaster, AL). Doxylstearic acid spin labels were purchased from Molecular Probes (Eugene, OR).

Preparation of DMPC/cholesterol membranes

The membranes used in this work were multilameller dispersions of DMPC containing 1 mol % spin labels (*n*-PC), T-PC, or *n*-SASL, and various amounts of cholesterol from 0 to 50 mol %, which we call the bulk cholesterol mole fraction. The membranes were prepared by the following method (44): chloroform solutions of DMPC and *n*-PC or *n*-SASL and cholesterol were mixed (containing 0.5×10^{-5} mol of total lipids), the chloroform was evaporated with a stream of nitrogen gas, and the lipid film on the bottom of the test tube was thoroughly dried under reduced pressure (~0.1 mm Hg) for 12 h. A buffer solution (0.2 ml of 10 mM PIPES and 150 mM NaCl, pH 7.0) was added to the dried lipids at 40°C and vigorously mixed on a vortex. The buffer used for the study samples with *n*-SASLs was 0.1 M borate at pH 9.5. A rather high pH was chosen in this case to ensure that all SASL probe carboxyl groups were ionized in the DMPC membranes (46–48).

Saturation recovery EPR

The DMPC or DMPC/cholesterol membranes were centrifuged briefly, and the loose pellet (~20% lipid, w/w) was used for the EPR measurements. The sample was placed in a capillary (0.6 mm i.d.) made of a gas-permeable polymer, TPX (49,50). For measurements of OTP, concentration of oxygen in the sample was controlled by equilibration with the same gas used for the temperature control, i.e., a controlled mixture of nitrogen and dry air adjusted with flowmeters (Matheson Gas Products model 7631H-604) (38,49,50). In all EPR measurements, the temperature was monitored using a copper-constantan thermocouple placed in the sample just above the active volume of the resonator.

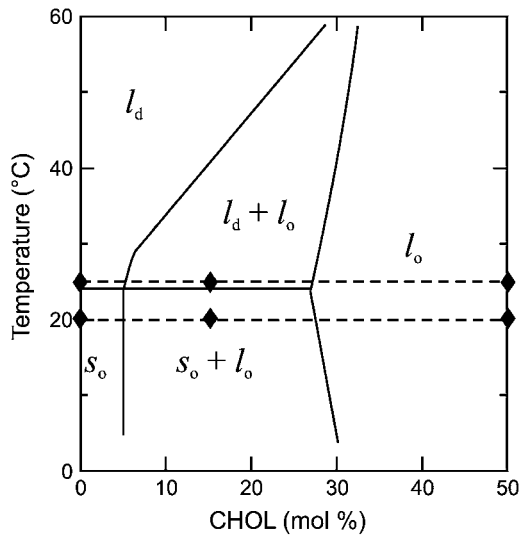

FIGURE 2 The phase diagram of the DMPC/cholesterol membrane, adapted from Almeida et al. (45). The broken lines indicate the DMPC/cholesterol mixtures and temperatures mainly addressed in the present work. Solid diamonds indicate lipid compositions and temperatures for which OTP profiles presented in Fig. 7 were obtained.

The T_1s of the spin labels were determined by analyzing the saturation recovery signal of the central line obtained by short-pulse saturation recovery EPR at X-band with the use of a loop-gap resonator (26,27,33,51). The saturation-recovery spectrometer was described previously (27,51). See also a recent review on saturation recovery by Hyde (52). The microwave field for short pulse experiments was 2.0 G (1 G = 10^{-4} T), and the pulse length was 0.3 μs. To avoid artificial shortening in T_1 measurement, a relatively low level of observing power (8 μW, with the loop-gap resonator delivering an H_1 field of 3.6×10^{-5} G) was used for all experiments. Typically 10^5–10^6 decays were acquired with 2048 data points on each decay. Sampling intervals were 2, 4, 8, 16, or 32 ns depending on sample, temperature, and oxygen tension. The total accumulation time was typically 2–5 min. Saturation-recovery curves were fitted by single or double exponential functions. When the single exponential fit was satisfactory, the decay time constant could be evaluated with a standard deviation smaller than ±5% from the mean value for independent experiments (for samples prepared independently). When the double exponential fit was necessary and satisfactory, the decay times were usually evaluated with standard deviations less than ±5% and ±30% for the longer and shorter recovery time constants, respectively (for independent samples and EPR measurements, these were the worst values in the measurements reported for this article). The large standard deviation for the shorter component resulted from the difficulty in measuring very short T_1s caused by the presence of molecular oxygen in the present setting of the instrument. In Figs. 4–6, we only indicated maximal errors.

The conventional EPR spectrum was routinely recorded for each sample, equilibrated with nitrogen gas. Remarkably, these conventional EPR spectra exhibited no clearly visible conventional features for the presence of two components, although Chiang et al. (53) and Swamy et al. (54) successfully carried out a nonlinear least-squares analysis of conventional EPR spectra, found the coexisting liquid-ordered and liquid-disordered domains in model membranes made from ternary lipid mixtures, and evaluated order parameters and reorientational diffusion coefficients in both of the coexisting domains. Their method is sensitive to the dynamic processes occurring in the time scale up to ~100 ns, whereas our method, which is based on spin-label T_1s, has a time window of 0.1–100 μs. Our present work is consistent with our earlier conventional EPR studies of PC/cholesterol membranes (44), suggesting that, without special analysis, the features of two coexisting domains cannot be evaluated separately. It further demonstrates that the DOT method is an excellent way of clearly discriminating and characterizing two coexisting domains (phases) in these lipid bilayers.

Outline of theory for the study of membrane domains using OTP

The effect of oxygen on the spin-lattice relaxation of spin labels is generally much greater than the motional effects (38). Thus, OTP, $W(x)$, was introduced as a convenient quantitative measure of the rate of the collision between the spin probe and molecular oxygen by Kusumi et al. (38) as:

$$W(x) = T_1^{-1}(\mathrm{Air}, x) - T_1^{-1}(\mathrm{N_2}, x) \quad (1)$$

where the T_1s are the spin-lattice relaxation times of the nitroxides in samples equilibrated with atmospheric air and nitrogen, respectively. The collision rate is also proportional to the local oxygen concentration, $C(x)$, and the local oxygen diffusion coefficient, $D(x)$ (thus, it is called the ''transport'' parameter and has nothing to do with active transport across the membrane), at a ''depth'' x in the membrane that is in equilibrium with atmospheric air.

$$W(x) = AC(x)D(x),\ A = 8\pi p r_o \quad (2)$$

where r_o is the interaction distance between oxygen and the nitroxide moiety of spin label (4.5 Å) (55), and p is the probability that an observable event occurs when a collision does occur (A is remarkably independent of the hydrophobicity and viscosity of the solvent and of spin label species) (49,56,57).

When the liquid-ordered and disordered domains are located in two different membrane domains, the spin label alone most often cannot differentiate between these domains, giving nearly indistinguishable conventional EPR spectra and similar T_1 values. However, even small differences in the lipid packing of these domains will affect oxygen partitioning and oxygen diffusion, which can be easily detected by observing the different T_1s from spin labels in these two locations in the presence of oxygen. In membranes equilibrated with air and consisting of two lipid environments with different oxygen transport rates, a fast oxygen transport (FOT) domain and a slow oxygen transport (SLOT) domain, the saturation-recovery signal is a simple double-exponential curve with time constants of T_1^{-1} (Air, FOT) and T_1^{-1} (Air, SLOT) (34,35).

$$W(\text{FOT}) = T_1^{-1}(\text{Air, FOT}) - T_1^{-1}(\text{N}_2\text{, FOT}) \quad (3)$$

$$W(\text{SLOT}) = T_1^{-1}(\text{Air, SLOT}) - T_1^{-1}(\text{N}_2\text{, SLOT}). \quad (4)$$

Here, ''x'' from Eq. 1 has been replaced by the two membrane domains FOT and SLOT, with a fixed depth (the same spin label is distributed between the FOT and SLOT domains). W(FOT) and W(SLOT) are OTPs in each domain and represent the collision rates in samples equilibrated with air. In the present work, we demonstrated that the DOT method can distinguish liquid-ordered, liquid-disordered, and solid-ordered domains in DMPC/cholesterol mixtures.

RESULTS AND DISCUSSION

Saturation recovery measurements and evaluation of OTP

Chemical structures of the spin labels used in this study, together with their approximate depth locations in the DMPC/cholesterol bilayer, are illustrated in Fig. 1. The majority of observations were carried out at 25°C and 20°C. As shown by broken lines in the phase diagram in Fig. 2, these temperatures are close to a phase boundary when the bulk cholesterol mole fraction is below 30 mol %, and the domain behaviors at these temperatures are interesting. All T_1 values were determined by analyzing the saturation-recovery signals for samples equilibrated with different partial pressures of oxygen.

Fig. 3 shows representative saturation recovery curves of 5-PC. In the bilayers containing 0 or 50 mol % cholesterol (A and B, both at 25°C), the saturation recovery signals were satisfactorily fit to a single exponential function in both the absence and presence of molecular oxygen (in nitrogen and 50% air, respectively; see the plots of residuals). In contrast, for the bulk cholesterol mole fraction of 15 mol % (C, D, and E observed at 25°C; F, G, and H observed at 20°C), the saturation recovery curves in the presence of molecular oxygen can be fit successfully only with double exponential curves (compare the residual in D (G) with that in E (H)), whereas single-exponential fit was satisfactory in the absence of molecular oxygen (for a sample equilibrated with nitrogen). These results are consistent with the presence of two phases under these conditions in the phase diagram shown in Fig. 2: the DMPC bilayer with an overall cholesterol content of 15 mol % contains l_o (liquid-ordered phase) and l_d (liquid-disordered phase) at 25°C, and l_o (liquid-ordered phase) and s_o (gel phase) at 20°C. Namely, although saturation recovery signal in the absence of molecular oxygen cannot differentiate the two phases, in the presence of oxygen, the recovery curves are very different between the two phases. This indicates that the collision rate of molecular oxygen, or OTP, is quite different in these two domains, consistent with the results by Ashikawa et al. (34). Likewise, the single-exponential recovery in A and B (0 and 50 mol % cholesterol, respectively) observed at 25°C is also consistent with the phase diagram in Fig. 2, indicating the presence of a single phase under these conditions.

In Fig. 4, T_1^{-1} values estimated for 5-PC in bilayers with an overall cholesterol content of 0, 15, and 50 mol % cholesterol at 25°C are plotted as a function of oxygen concentration (as percentage air in the air-nitrogen mixture) in the equilibrating gas mixture. All of the plots exhibited a linear dependence on percentage air. In fact, all of the T_1^{-1} plots for all of the spin probes used in this work at both 20°C and 25°C showed linear dependences on the oxygen concentration between 0 and 50% air. This did not happen in the influenza envelope membrane, representing a fast exchange of the probes between the two domains (the domains enriched in both hemagglutinin and cholesterol and the bulk domain) or rapid continual formation and disintegration of the protein-cholesterol-rich domains (35). Therefore, the linear dependence of T_1^{-1} on oxygen concentration in these plots indicates that the exchange rate of spin-labeled lipids between the two coexisting domains is slow ($<10^4$ s^{-1}, the upper time window limit of the DOT method (35)) or the lifetime of each domain is long (longer than 100 μs), probably because both domains are large (34,35). Assuming the diffusion coefficient of spin probes to be 9 μm^2/s (58), over 100 μs, they would cover an area of ~60 nm in radius (square root of $4 \times 9\ \mu\text{m}^2/\text{s} \times 100\ \mu\text{s}$), suggesting that the domain size is at least 60 nm in radius.

$W(x)$, the OTP, can be obtained by extrapolating the linear plot to the sample equilibrated with the atmospheric air (see Eq. 1 and Kusumi et al. (38); this process was required because the accurate observation of saturation recovery becomes increasingly difficult as the oxygen partial pressure is increased as a result of faster recoveries). To assign the two OTPs to the two phases in the phase diagram, we assumed that the OTP in the liquid-ordered domain was greater than that for the gel phase and smaller than that for the liquid-disordered phase (59). (Because the preexponential factors in the fitting of the recovery curves are not robust parameters, we were unable to correlate the apparent populations of fast- and slow-recovering components to the populations of the two phases.)

An unexpected finding is that the oxygen collision rate at the 5-PC position is greater in the l_d-phase domains that exist

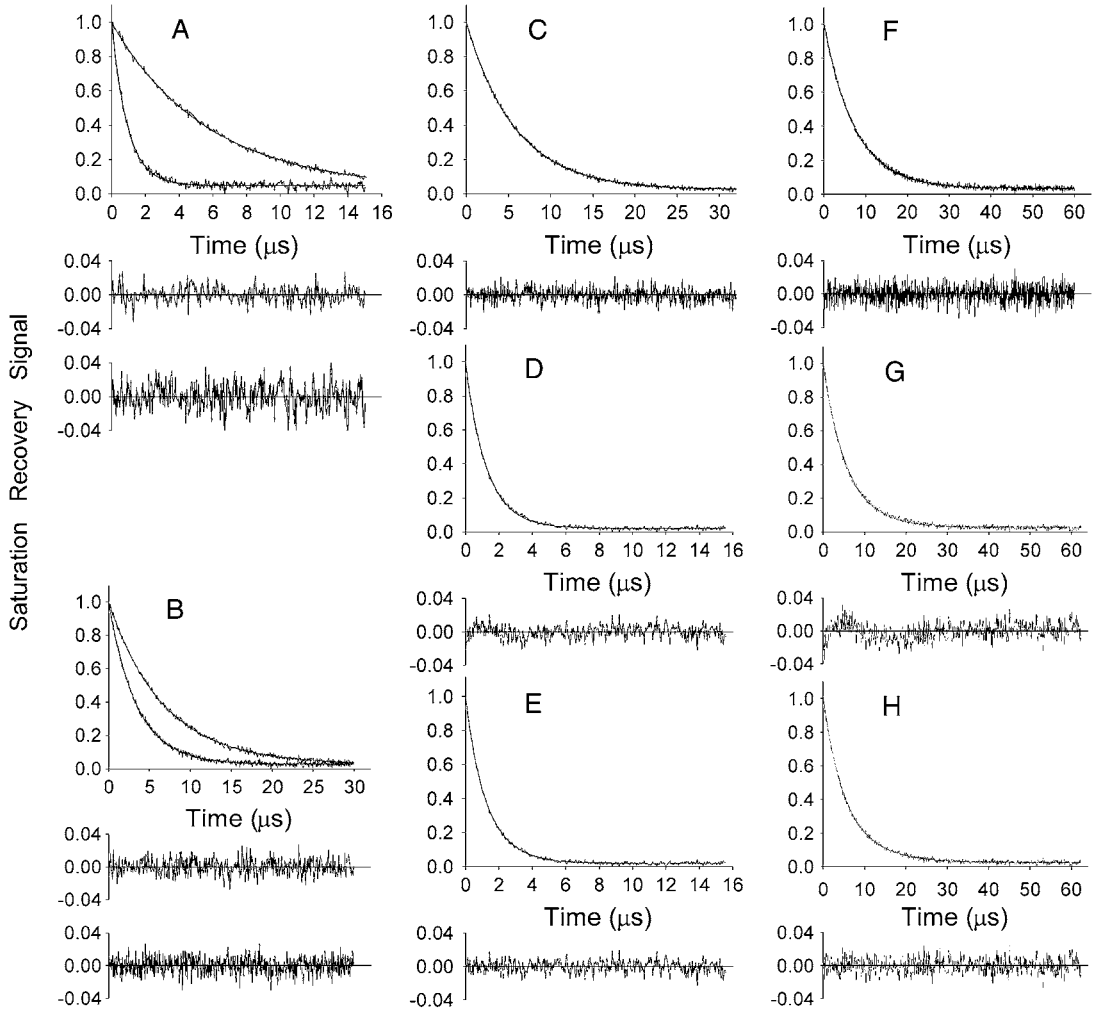

FIGURE 3 Representative saturation-recovery signals with fitted curves and the residuals (the experimental signal minus the fitted curve) of 5-PC in DMPC-cholesterol bilayers, obtained at 25°C (*A–E*) and 20°C (*F–H*). The membrane specimens were equilibrated with nitrogen (*A top, B top, C, F*) or the mixture of 50% air and 50% nitrogen (*A bottom, B bottom, D, E, G, H*). The overall cholesterol content (the mixing ratio) in the membrane was 0 (*A*), 50 (*B*), and 15 (*C–H*) mol %. Experimental data were fitted either to single exponentials with time constants of 5.73 μs (*A top*), 0.93 μs (*A bottom*), 6.72 μs (*B top*), 3.42 μs (*B bottom*), 5.82 μs (*C*), 1.27 μs (*D*), 2.40 μs (*F*), and 3.87 μs (*G*), or double exponentials with time constants of 1.38 μs and 0.61 μs (*E*), 3.84 μs and 1.93 μs (*H*). For 15 mol % overall cholesterol in the presence of oxygen, the search to fit to a single exponential function was unsatisfactory (*D* and *G*, see the residuals), requiring a double-exponential fitting (*E* and *H*). The double-exponential fit is consistent with the presence of two immiscible phases (domains) with different oxygen transport rates.

in the membrane with an overall cholesterol content of 15 mol % (from the phase diagram in Fig. 2, this domain actually contains ~5 mol % cholesterol) than that in the l_d-phase domains (the entire membrane) of the pure DMPC bilayer. We return to this point later in this article.

Temperature dependence of OTP across the phase boundaries

In Fig. 5, OTP obtained with 5-PC and 14-PC in DMPC membranes containing three different bulk cholesterol mole fractions (0, 15, and 50 mol %) is plotted as a function of temperature, indicating single (for 0 mol % cholesterol, Fig. 5, *A* and *D*, and 50 mol % cholesterol, Fig. 5, *C* and *F*) and double (for 15 mol % cholesterol, with the exception of data at 45°C where single exponential fit was obtained indicating the presence of only the FOT component, Fig. 5, *B* and *E*) exponential fits. These data indicate that for both locations the lipid environment is homogeneous in terms of oxygen transport in the 0.1- to 100-μs range for pure DMPC (s_o phase below and l_d phase above the phase transition temperature) and in the presence of 50 mol % cholesterol (l_o phase below and above the phase transition temperature). DMPC membranes with a bulk cholesterol mole fraction of 15 mol % exhibit two domains with different oxygen transport rates. Below the phase transition temperature, we attributed these domains to the l_o phase and s_o phase, and above the phase transition temperature to the l_o phase and l_d phase.

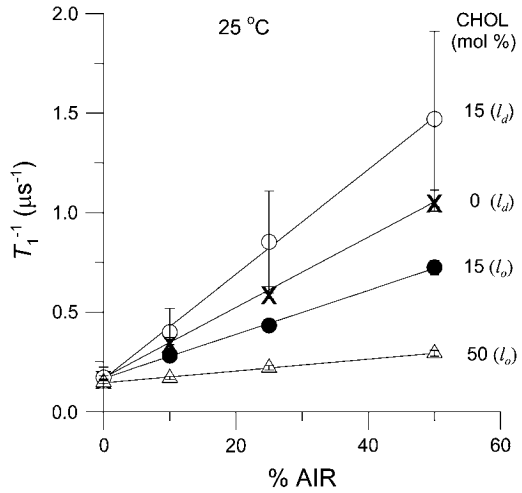

FIGURE 4 T_1^{-1} for 5-PC in various domains of DMPC/cholesterol membranes at 25°C, plotted as a function of the fraction of air in the equilibrating gas mixture. DMPC membranes with no cholesterol (×, l_d phase), 15 mol % overall cholesterol (*solid circle*, l_o phase; *open circle*, l_d phase), and 50 mol % overall cholesterol (*open triangle*, l_o phase). The error bars represent the maximal deviations (see the Saturation recovery EPR subsection in the Materials and Methods section).

However, at 45°C only one phase was found, which we attributed to the l_d phase based on the phase diagram (Fig. 2) and dependences shown in Fig. 5, *B* and *E*. The abrupt change of the OTP observed in the absence of cholesterol at the main phase transition temperature (Fig. 5, *A* and *D*) is abolished by the presence of 50 mol % cholesterol for both locations, close to the membrane surface (5-PC) and in the membrane center (14-PC). It is worth noticing that at 50 mol % cholesterol, the OTP at 5-PC position (and wide temperature region below and above the phase transition) is close to that in the pure DMPC gel-phase membrane. Similarly, at 50 mol % cholesterol, the OTP at 14-PC position is practically the same as that in the pure fluid-phase DMPC membrane in a broad temperature range.

At a bulk cholesterol mole fraction of 15 mol %, where two coexisting domains are present, the picture is complex (Fig. 5, *B* and *E*). With a rise in temperature, at the main phase transition temperature, the SLOT component disappears, and an FOT component appears, whereas the oxygen-transport parameter of the other component changes gradually and continuously across the main phase transition temperature. This was observed with both 5- and 14-PC. Based on the phase diagram shown in Fig. 2, this result suggests that the s_o domain with low OTP present below the phase transition temperature is converted to the l_d domain with high OTP, whereas the l_o domain is rather stable, giving the OTP in the l_o domain gradual changes, even across the main phase transition temperature of DMPC. Such phase behavior (s_o turns into l_d, whereas l_o changes gradually across the DMPC phase transition temperature) was expected, particularly because the related phase boundaries are almost vertical. To the best of our knowledge, this was the first time that such changes have been directly observed.

In addition, Fig. 5 shows an important feature of the l_d domain that contains small amounts of cholesterol (~5 mol %). Its OTPs with both 5- and 14-PC are greater than those in the l_d domain containing no cholesterol. This tendency is stronger with 14-PC, i.e., in the middle of the bilayer. We return to this point in our discussion of Figs. 6 and 7.

How much is the OTP in the liquid-ordered domain affected by the surrounding liquid-disordered or solid-ordered domains?

In Fig. 6, the OTPs measured at 20°C and 25°C using 5-PC (near the membrane surface) and 14-PC (near the central part of the membrane) are plotted as a function of the overall cholesterol content. The results shown in Fig. 6 indicate a large scattering of points for the OTP in the l_d domain, in particular that containing cholesterol, which is probably a result of very short T_1s measured in the l_d domain in the presence of oxygen. Further evaluation of the error is given in the Materials and Methods section. According to the phase diagram shown in Fig. 2, the variations of the overall cholesterol content between ~5 and ~27 mol % will affect the fractions of l_o and s_o (20°C, each phase contains constant mole fractions of 27% and 5% cholesterol, respectively) and l_o and l_d (25°C, each phase again contains constant mole fractions of 27% and 5% cholesterol, respectively), whereas in overall cholesterol mole fractions between 0 and ~5%, the phases remain s_o (20°C) and l_d (25°C) (in both phases, the cholesterol mole fraction is the same as the experimental mixing ratio), and in those between 30% and 50%, the phase remains l_o at both temperatures (at both temperatures, the cholesterol mole fraction is the same as the experimental mixing ratio). The major interest here is whether l_o domains show different characteristics in terms of the oxygen collision rate when they are in equilibrium with the l_d or s_o phase.

At a bulk cholesterol mole fraction between 30 and 50 mol %, the OTP is slightly greater at 25°C than at 20°C, suggesting a small temperature-dependent increase of the OTP in the l_o phase when the temperature is raised from 20°C to 25°C. At the bulk cholesterol mole fraction of 10%, ~23% of cholesterol is in the l_o phase (both at 20°C and 25°C) and 77% in the s_o and l_d phases (at 20°C and 25°C, respectively); here, 5-PC indicated that the OTP in the l_o phase is greater when it is surrounded by the l_d phase than by the s_o phase—to an extent greater than expected from the temperature-dependent changes. This was also observed for lower bulk cholesterol mole fractions and in a less marked way with 14-PC located in the middle of the membrane. This influence of the surrounding domain (l_d or s_o phases) may be caused either by the bulk effect of the surrounding domain (with different oxygen concentrations) or by the different properties of the domain boundaries. In either case, data suggest that the l_o domain is small.

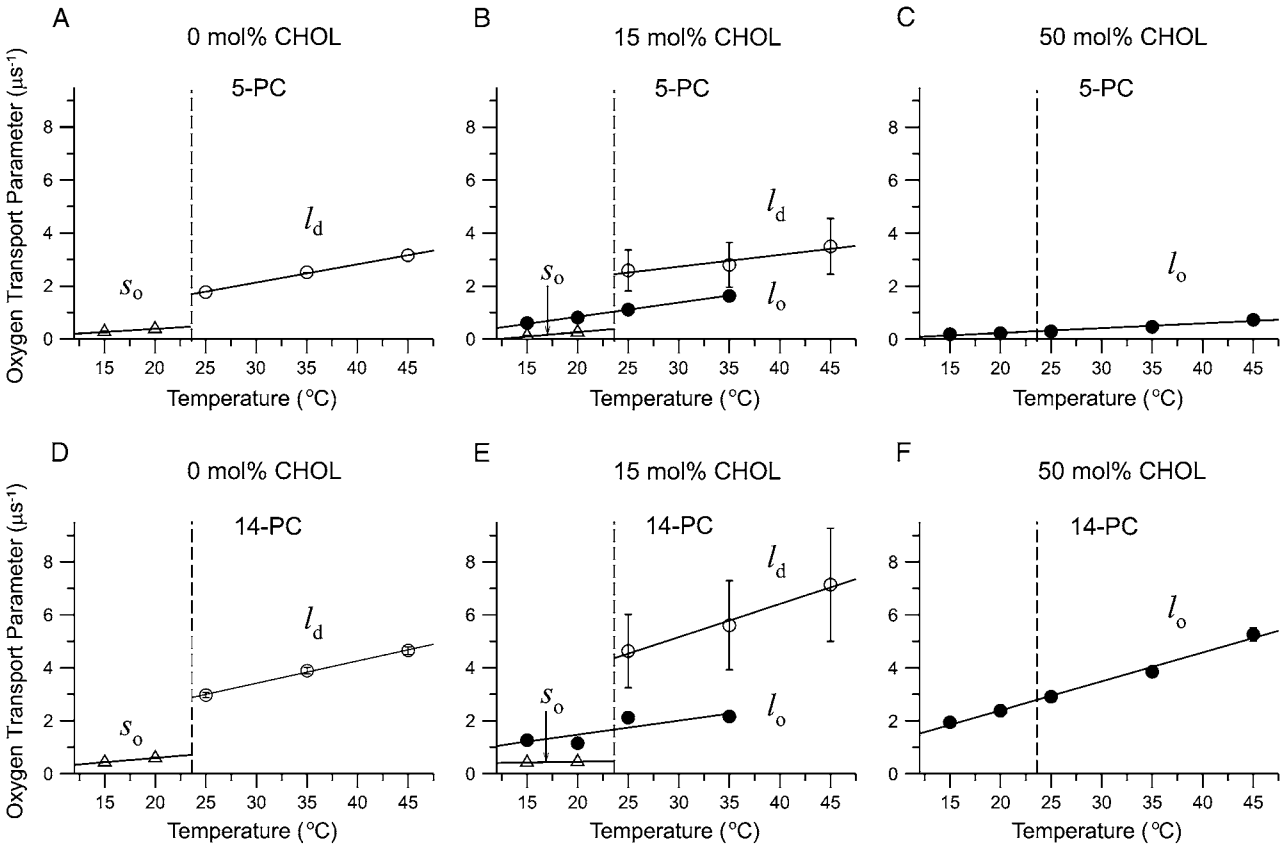

FIGURE 5 OTPs obtained with 5- and 14-PC in DMPC/cholesterol membranes containing 0, 15, and 50 mol % overall cholesterol, plotted as a function of temperature. The vertical dashed line at 23.6°C shows the phase transition temperature of the pure DMPC bilayer. Two OTPs obtained for the membranes containing 15 mol % overall cholesterol represent those for l_o (*solid circle*) and s_o (*open triangle*) phases below the phase-transition temperature and l_o (*solid circle*) and l_d (*open circle*) phases above the phase-transition temperature (also indicated in the figure). The error bars represent the maximal deviation (see the Saturation recovery EPR subsection in the Materials and Methods section).

To evaluate the upper limit of the l_o domain size, let us assume that the influence of adjacent domains in a different phase can be detected when one-third of the l_o domain area is under the influence of the adjacent domains (or the boundary region is greater than one-third of the l_o domain size). Assuming that the diffusion coefficient of molecular oxygen in the l_o domain is ~300 $\mu m^2/s$ (three times less than that in the bulk DMPC domain; for the evaluation of the oxygen diffusion coefficient in the DMPC bilayer at 25°C, see Windrem and Plachy (55) and Subczynski and Hyde (60,61)) during the spin-lattice relaxation time of 10 μs, molecular oxygen would cover an area of 135 nm in radius (oxygen diffusion is three-dimensional diffusion). This leads to a simplistic equation of $(a + 135)^2/a^2 = 1.3$, giving $a \approx 960$ nm. Hence, the upper estimate of the l_o domain radius is ~1000 nm.

The cholesterol content of the l_o phase in the membrane containing the overall cholesterol concentration between 5 and 20 mol % is nearly constant (~27 mol %) both at 20°C

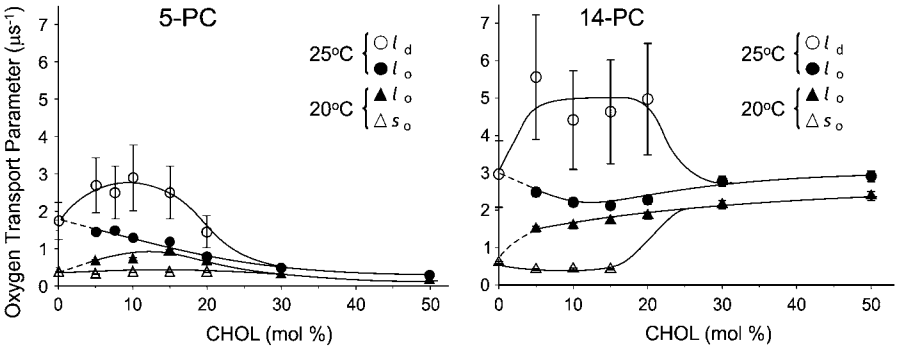

FIGURE 6 OTPs plotted as a function of the overall cholesterol content (mixing ratio). Data were obtained at 20°C (*open triangle*, s_o phase; *solid triangle*, l_o phase) and 25°C (*open circle*, l_d phase; *solid circle*, l_o phase) with 5-PC (*top*) and 14-PC (*bottom*). The error bars represent the maximal deviation (see the Saturation recovery EPR subsection in the Materials and Methods section).

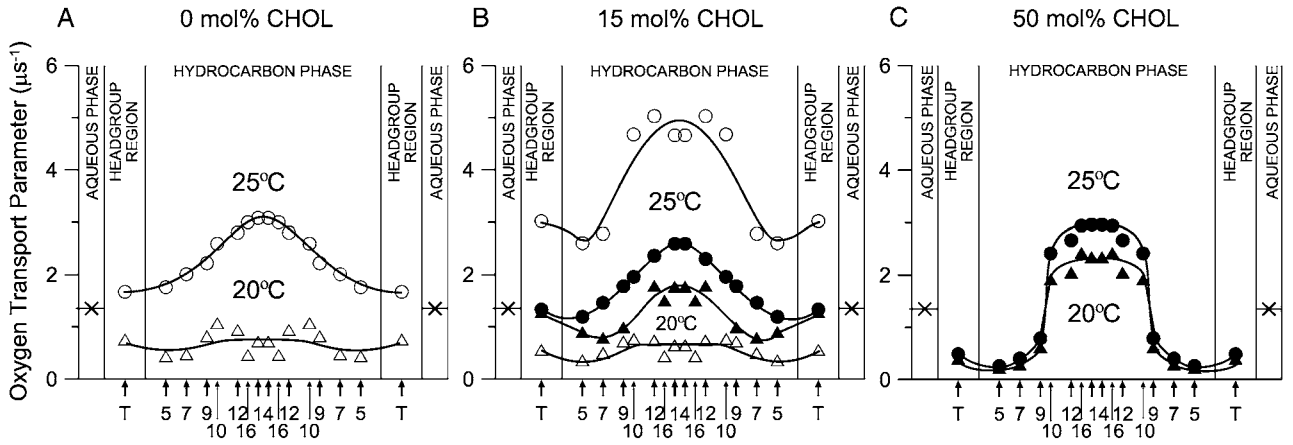

FIGURE 7 Profiles of OTP (oxygen diffusion-concentration product) across DMPC-cholesterol bilayers. The parameters for the l_o domains are shown by solid keys, and those for l_d and s_o domains are shown in open keys. (*A*) 0 mol % cholesterol: (*open circle*) l_d domains at 25°C, (*open triangle*) s_o domains at 20°C. (*B*) 15 mol % overall cholesterol: (*open circle*) l_d domain at 25°C, (*solid circle*) l_o domain at 25°C, (*solid triangle*) l_o domain at 20°C, (*open triangle*) s_o domain at 20°C. (*C*) 50 mol % overall cholesterol: (*solid circle*) l_o domain at 25°C, (*solid triangle*) l_o domain at 20°C. Arrows indicate approximate locations of nitroxide moieties of spin labels. T indicates T-PC. The symbol × indicates OTP in the aqueous phase (35). It does not change significantly because the temperature dependences of oxygen diffusion and concentration are opposite. Values of OTPs obtained with *n*-PC and *n*-SASL with the same *n* are practically the same. Lipid compositions and temperatures for which these profiles were obtained are indicated in the phase diagram presented in Fig. 2 as solid diamonds.

and 25°C, as depicted in the phase diagram in Fig. 2, and we anticipate that the OTP for the l_o domain in this overall cholesterol concentration range is comparable to that for 30 mol % cholesterol. However, there is a slight dependence of the OTP for the l_o domain on the overall cholesterol concentration in the range of 5–20 mol % for both 5-PC and 14-PC at both temperatures. This suggests that, in this cholesterol range, not only do changes of the relative amounts of l_o and l_d (or s_o) phases take place, but also the size of the individual l_o-phase domain increases, reducing the effects of surrounding l_d or s_o phases.

How can we reconcile the domain size evaluated in the present research (the lower limit of 60 nm and the upper limit of 1000 nm) and those found in fluorescent microscopy, which reports the size of micrometer to several 10 s of micrometers (62–69)? First, because giant unilamellar liposomes cannot be formed with the present binary mixture of DMPC and cholesterol, the l_o domain size of this mixture may be much smaller than those sizes found in mixtures used in the fluorescence microscopy research. Second, in the research using giant unilamellar vesicles, there generally exist many smaller liposomes that were not used for the observation, and these smaller liposomes must have much smaller l_o domains. Third, the large l_o domains observed under the fluorescence microscope may be clusters of these smaller l_o domains that were in fact separated by small or thin l_d- or s_o-phase domains but that could not be detected because of the lack of spatial resolution (~300 nm). In fact, to the best of our knowledge, no evaluation of the lipid composition in the apparent l_o domain in the giant unilamellar liposome being observed under the fluorescence microscope exists in the literature (e.g., using time-of-flight mass spectroscopy combined with microscopic laser evaporation).

At the present time, we are unable to determine which of these possibilities may be correct, but the results obtained here illustrate the necessity to be cautious about the l_o domain size determined in artificial membranes using optical microscopy. In the raft literature, it is often assumed that, whereas the l_o domains of a size as large as 1–10 μm are found in artificial membranes, such an l_o-like domain cannot be seen in the cellular plasma membrane before the cells are stimulated extracellularly or queued intracellularly. Furthermore, an argument has been advanced that the absence of such domains in the plasma membrane may be a result of the complexity in the molecular compositions and the presence of membrane molecules that have detergent-like surface activity, making the raft smaller than the optical resolution of the microscope. However, our results suggest the possibility that even in artificial membranes, the true l_o domain size may be comparable to the optical diffraction limit or even smaller.

OTP profiles across the membrane

Transmembrane OTP profiles across the l_o-, l_d-, and s_o-phase domains in DMPC/cholesterol bilayers were obtained at 25°C and 20°C using nine lipid spin labels as shown in Fig. 1 and are displayed in Fig. 7 (*A*, without cholesterol; *B*, 15 mol % overall cholesterol; *C*, 50 mol % overall cholesterol). Lipid compositions and temperatures for which these profiles were obtained are indicated as solid diamonds in the phase diagram depicted in Fig. 2. The profiles in Fig. 7 *A* are those for l_d- and s_o-phase domains that contain no cholesterol. It is

somewhat surprising that OTPs of these domains differ only by a factor of two to four at all depths.

Profiles in the l_o domains in different surroundings were obtained in the three distinct regions in the phase diagram (*solid keys* in Fig. 7, *B* and *C*): 1), the l_o domain that coexists with the l_d domain (27 mol % cholesterol in the domain for 15 mol % overall cholesterol at 25°C; Fig. 7 *B*); 2), the l_o domain that coexists with the s_o domain (27 mol % cholesterol in the domain for 15 mol % overall cholesterol at 20°C; Fig. 7 *B*); and 3), the l_o phase that constitutes the whole membrane (50 mol % overall cholesterol at 25°C and 20°C; both are within the same phase region; Fig. 7 *C*). At 15 mol % overall cholesterol at both temperatures (25°C and 20°C, Fig. 7 *B*), both l_d and s_o domains contain 5 mol % cholesterol, whereas l_o domains contain 27 mol % cholesterol. In this cholesterol concentration range, the overall shape of the OTP profiles across the membrane remains the same, although actual values greatly vary in different domains. The profiles for the l_o domains lie between those of l_d and s_o domains, as expected.

However, we were amazed to find that the profile for the l_o domain, containing 27 mol % cholesterol (Fig. 7 *B*), is not so much different (only 20–40%) from that for the l_d domain, which does not contain any cholesterol (Fig. 7 *A*; both observed at 25°C). Further increase in the overall cholesterol content to 50 mol %, which makes the whole membrane an l_o phase, induced a dramatic change of the OTP profile, both at 25°C and 20°C (Fig. 7 *C*). It decreased the OTP close to the membrane surface and increased it in the membrane center, resulting in a sharp three- to fourfold change in the OTP between the C-9 and C-10 positions, making the profile almost rectangular. The overall change of the OTP across the membrane is as large as a factor of ~15: values of the OTP at depths close to the membrane surface become as low as those observed in the s_o domain, and those in the membrane center as high as those observed for the l_d domain in the absence of cholesterol. The abrupt increase of OTP occurs at the depth to which the rigid tetracyclic cholesterol structure is immersed (31,33,68–71).

These results suggest that the liquid-ordered domain made of saturated phospholipids and cholesterol may be ordered only near the membrane surface, retaining high disorder in the middle of the membrane. This property may help the l_o domain to retain high lateral mobility of incorporated molecules within the domain. To explain the OTP profiles in the l_o-phase domains, consider cholesterol localization in the lipid bilayer membrane. The rigid plate-like tetracyclic ring structure of cholesterol reaches the depth of C-7 to C-10 in the lipid bilayer, and the cholesterol isooctyl chain with the cross section much smaller than that of the rigid ring is located in the membrane center (70). This would produce free volume in the membrane center, where *gauche-trans* conformational changes of the alkyl chains as well as oxygen transport may be enhanced. For further discussion, refer to our previous articles (31,33,71). Interestingly, the hydrophobicity profile across the DMPC/cholesterol (50/50 mol fraction) membrane exhibited an abrupt increase in hydrophobicity between the C-9 and C-10 positions toward the membrane center (71).

In addition, comparison of the OTP in the l_d domain that contains no cholesterol (*upper graph* in Fig. 7 *A*) with that in the l_d domain containing 5 mol % cholesterol (*upper graph* in Fig. 7 *B*) reveals that the OTP is much greater in the l_d domain, which contains very small concentrations (5 mol %) of cholesterol throughout all membrane depths (*upper graph* in Fig. 7 *B*: this result was also apparent in the data shown in Figs. 4–6). This is surprising not only because it is contrary to the general view that cholesterol increases the alkyl chain order and suppresses the molecular motion but also because such a small concentration of cholesterol induced such large increases (up to ~60%, which occurs in the bilayer central region) in the OTP. However, we previously showed that small amounts of cholesterol (<5 mol %) increase the alkyl chain mobility (*gauche-trans* isomerization) in the l_d phase (see Fig. 3 in Subczynski and Kusumi (72)). There, a strong rigidifying effect of cholesterol was observed only for cholesterol concentrations above 5 mol %. This enhanced mobility of 5-SASL and the OTP in the presence of very small amounts of cholesterol may be caused by the cholesterol's impurity effect to destroy the cooperative dynamic characteristics by forming the membrane of a single molecular species, which is particularly apparent in the middle of the bilayer because cholesterol induces vacant space there.

Another apparent contradiction to the common belief of cholesterol's ''ordering or rigidifying effect'' is found in the middle of the l_o-phase bilayer in the presence of 50 mol % cholesterol (Fig. 7 *C*). The OTP values in the positions C-12, C-14, and C-16 are greater than those in the l_o-phase domain containing 27 mol % cholesterol (*second graph from the top* in Fig. 7 *B*) or even those in the l_d-phase bilayer without cholesterol (*top graph* in Fig. 7 *A*). Again, this is probably because there is more free volume in the central part of the bilayer created by the presence of cholesterol, which is much bulkier in the planar tetracyclic ring structure than its alkyl chain part (31,33). Because molecular oxygen is a very small probe, the OTP is likely to be a very sensitive monitor for the creation of such small and dynamic free space in the central part of the bilayer.

Liquid-ordered domains present in the liquid-disordered membrane appear to be made of two matched l_o domains in both leaflets of the bilayer (6,65,67,73). Generally, fluorescence microscopy observations of the bilayers containing these domains have reported the presence of two clearly separated domains, l_o and l_d domains, and not the presence of regions where the l_o domain in one leaflet overlaps with the l_d domain in the other leaflet. These results suggest that to coexist stably with the l_d domain, the l_o domain tends to be stabilized in some way by matching the ordered domains in both leaflets and enhancing the coupling of the two layers

through interdigitated lipids (1,6,9,74). Thus, we assume that the obtained profiles reflect the bilayer property rather than the property of the l_o domain in each leaflet.

GENERAL DISCUSSION

The phase diagrams available for the binary mixtures of DMPC and cholesterol indicate the regions of the lipid composition and temperature in which different phases coexist (15,42–45). The present research was undertaken to characterize the physical properties of the l_o-phase domain under the conditions where two phases coexist. Previously, such characterization has mostly been limited to the membranes that solely consist of a single phase (75–80). We found that the commonly accepted statement that the properties of the liquid-ordered-phase domains lie between those for the liquid-disordered and solid-ordered domains (59) is true for membranes containing bulk cholesterol mole fractions below 27% where the l_o domain coexists with the l_d or s_o domain. However, at higher cholesterol concentrations, the OTP in the l_o domain is like that in the s_o domain near the membrane surface (from the surface to the depth of C-9) and like that in the l_d domain in the central region of the membrane (at depths deeper than C-9).

Conventional EPR at X-band was used some time ago to indicate coexisting phases in the binary mixtures of phosphatidylcholine and cholesterol, giving evidence for the existence of the immiscible fluid phases (liquid-ordered and liquid-disordered) (42–44). More recently, high-frequency EPR was employed to study faster reorientational motion (75,81,82). In the present study, to gain more insight regarding the dynamics in the cholesterol-rich domains, a pulse EPR T_1 method was used. Because it is more sensitive to membrane dynamics at longer time-space scales than other EPR and fluorescence techniques, it is thought to be suitable for the studies of the dynamics occurring in the liquid-ordered phase. Using the DOT method, which can cover the membrane dynamics in the range from 0.1 to 100 μs, we carried out extensive characterizations of the three-dimensional structure of the l_o domain, with special attention paid to the molecular dynamics and structures in the third dimension, namely, in the depth direction in the membrane.

The only measurement of the OTP in the raft domain in the biological membranes was that reported for the influenza virus membrane at the depth of carbon C-14 (35). The OTP exhibited an extremely low value, 16 times lower than that observed in the surrounding bulk region or that observed in a lipid membrane made of the total lipid extract from the influenza virus. The major reason for such a low OTP in the raft domain in the influenza virus envelope membrane was proposed to be a very high concentration of cholesterol, of the order of 50 mol %, coupled with high concentrations of transmembrane proteins, hemagglutinin, and neuraminidase.

Previously, we obtained the profiles of the OTP across the reconstituted membranes containing various concentrations of bacteriorhodopsin (34). At high bacteriorhodopsin/lipid ratios, a domain where the oxygen transport is very slow, the SLOT domain, was formed. In the SLOT domain, the profile of the OTP was almost flat at very low values, similar to that observed in the purple membrane. Meanwhile, in the liquid-crystalline (l_d phase) 1-palmitoyl-2-oleoyl PC membrane containing model α-helical transmembrane peptides at a concentration of 10 mol %, the OTP was decreased by 20–30% (41) throughout all depths in the membrane, making the OTP in the l_d phase at 35°C very similar to that observed in the l_o domain in the DMPC-cholesterol membrane containing 15 mol % cholesterol at 25°C. These results indicate that the OTP profile across the membrane provides valuable information on the three-dimensional organization of membrane molecules in the microdomains in the membrane. Such knowledge has never been acquired by other methods and will be important for understanding the three-dimensional dynamic organizations of the membrane microdomains.

This work was supported by grants EY015526, EB002052, and EB001980 of the National Institutes of Health, and also by Grants-in-Aid for Scientific Research (General and on Priority Areas) from the Ministry of Education, Culture, Sport, Science, and Technology of Japan.

REFERENCES

1. Simons, K., and E. Ikonen. 1997. Functional rafts in cell membranes. *Nature*. 387:569–572.
2. Zurzolo, C., G. van Meer, and S. Mayor. 2003. The order of rafts. *EMBO Rep*. 4:1117–1121.
3. Subczynski, W. K., and A. Kusumi. 2003. Dynamics of raft molecules in the cell and artificial membranes: approach by pulse EPR spin labeling and single molecule optical microscopy. *Biochim. Biophys. Acta*. 1610:231–243.
4. Mayor, S., and M. Rao. 2004. Rafts, scale dependent, active lipid organization at the cell surface. *Traffic*. 5:231–240.
5. Mukherjee, S., and F. R. Maxfield. 2004. Membrane domains. *Annu. Rev. Cell Dev. Biol*. 20:839–866.
6. Kusumi, A., I. Koyama-Honda, and K. Suzuki. 2004. Molecular dynamics and interactions for creation of stimulation-induced stabilized rafts from small unstable steady-state rafts. *Traffic*. 5:213–230.
7. Kusumi, A., C. Nakada, K. Ritchie, K. Murase, K. Suzuki, H. Murakoshi, R. S. Kasai, J. Kondo, and T. Fujiwara. 2005. Paradigm shift of the plasma membrane concept from the two-dimensional continuum fluid to the partitioned fluid: high-speed single-molecule tracking of membrane molecules. *Annu. Rev. Biophys. Biomol. Struct*. 34: 351–378.
8. Kusumi, A., H. Ike, C. Nakada, K. Murase, and T. Fujiwara. 2005. Single-molecule tracking of membrane molecules: plasma membrane compartmentalization and dynamic assembly of raft-philic signaling molecules. *Semin. Immunol*. 17:3–21.
9. Simons, K., and W. L. C. Vaz. 2004. Model systems, lipid rafts, and cell membranes. *Annu. Rev. Biophys. Biomol. Struct*. 33:269–295.
10. Patel, R. C., U. Kumar, D. C. Lamb, J. S. Eid, M. Rocheville, M. Grant, A. Rain, T. Hazlett, S. C. Patel, E. Gratton, and Y. C. Patel. 2002. Ligand binding to somatostatin receptors induces receptor-specific oligomer formation in live cells. *Proc. Natl. Acad. Sci. USA*. 99:3294–3299.
11. Gaus, K., E. Gratton, E. P. W. Kable, A. S. Jones, I. Gelissen, L. Kritharides, and M. Jessup. 2003. Visualizing lipid structure and raft domains in living cells with two-photon microscopy. *Proc. Natl. Acad. Sci. USA*. 100:15554–15559.

12. Munro, S. 2003. Lipid rafts: elusive or illusive. *Cell*. 115:377–388.

13. Taner, S. B., B. Onfeld, N. J. Pirinen, F. E. McCann, A. J. Magee, and D. M. Davis. 2004. Control of immune responses by trafficking cell surface proteins, vesicles, and lipid rafts to and from the immunological synapse. *Traffic*. 4:651–661.

14. van Meer, G., and H. Sprong. 2004. Membrane lipids and vascular traffic. *Curr. Opin. Cell Biol*. 16:373–378.

15. Almeida, P. F. F., A. Pokorny, and A. Hinderliter. 2005. Thermodynamics of membrane domains. *Biochim. Biophys. Acta*. 1720:1–13.

16. Jacobson, K., and C. Dietrich. 1999. Looking at lipid rafts? *Trends Cell Biol*. 9:87–91.

17. Dietrich, C., B. Yang, T. Fujiwara, A. Kusumi, and K. Jacobson. 2002. Relationship of lipid rafts to transient confinement zones detected by single particle tracking. *Biophys. J*. 82:247–284.

18. Anderson, R. G., and K. Jacobson. 2002. A role for lipid shells in targeting proteins to caveolae, rafts, and other lipid domains. *Science*. 296:1821–1825.

19. Maxfield, F. R. 2002. Plasma membrane microdomains. *Curr. Opin. Cell Biol*. 14:483–487.

20. Baumgart, T., S. T. Hess, and W. W. Webb. 2003. Imaging coexisting fluid domains in biomembrane models coupling curvature and line tension. *Nature*. 425:821–824.

21. Rao, M., and S. Mayor. 2005. Use of Forster's resonance energy transfer microscopy to study lipid rafts. *Biochim. Biophys. Acta*. 1746: 221–233.

22. Sperotto, M. M., and O. G. Mouritsen. 1991. Monte Carlo simulation studies of lipid order parameter profiles near integral proteins. *Biophys. J*. 59:261–270.

23. Mouritsen, O. G., and M. J. Zuckermann. 2004. What's so special about cholesterol? *Lipids*. 39:1101–1113.

24. Zuckermann, M. J., J. H. Ipsen, L. Miao, O. G. Mouritsen, M. Nelsen, J. Polson, J. Thewalt, I. Vattulani, and H. Zhu. 2004. Modeling lipid-sterol bilayers: application to structural evolution, lateral diffusion, and rafts. *Methods Enzymol*. 383:198–229.

25. Merkle, H., W. K. Subczynski, and A. Kusumi. 1987. Dynamic fluorescence quenching studies on lipid mobilities in phosphatidylcholine-cholesterol membranes. *Biochim. Biophys. Acta*. 897:238–248.

26. Yin, J.-J., J. B. Feix, and J. S. Hyde. 1990. Mapping of collision frequencies for stearic acid spin labels by saturation-recovery electron paramagnetic resonance. *Biophys. J*. 58:713–720.

27. Yin, J.-J., and W. K. Subczynski. 1996. Effect of lutein and cholesterol on alkyl chain bending in lipid bilayers: a pulse electron paramagnetic resonance spin labeling study. *Biophys. J*. 71:832–839.

28. Zaccai, G., G. Büldt, A. Seelig, and J. Seelig. 1979. Neutron diffraction studies on phosphatidylcholine model membranes II. Chain conformation and segmental disorder. *J. Mol. Biol*. 134:693–706.

29. Träuble, H. 1971. The movement of molecules across lipid membranes: a molecular theory. *J. Membr. Biol*. 4:193–208.

30. Pace, R. J., and S. I. Chan. 1982. Molecular motions in lipid bilayers. III. Lateral and transversal diffusion in bilayers. *J. Chem. Phys*. 76: 4241–4247.

31. Subczynski, W. K., J. S. Hyde, and A. Kusumi. 1991. Effect of alkyl chain unsaturation and cholesterol intercalation on oxygen transport in membranes: a pulse ESR spin labeling study. *Biochemistry*. 30:8578–8590.

32. Altenbach, C., D. A. Greenhalgh, H. G. Khorana, and W. L. Hubbell. 1994. A collision gradient method to determine the immersion depth of nitroxides in lipid bilayers: application to spin-labeled mutants of bacteriorhodopsin. *Proc. Natl. Acad. Sci. USA*. 91:1667–1671.

33. Subczynski, W. K., J. S. Hyde, and A. Kusumi. 1989. Oxygen permeability of phosphatidylcholine-cholesterol membranes. *Proc. Natl. Acad. Sci. USA*. 86:4474–4478.

34. Ashikawa, I., J.-J. Yin, W. K. Subczynski, T. Kouyama, J. S. Hyde, and A. Kusumi. 1994. Molecular organization and dynamics in bacteriorhodopsin-rich reconstituted membranes: Discrimination of lipid environments by the oxygen transport parameter using a pulse ESR spin-labeling technique. *Biochemistry*. 33:4947–4952.

35. Kawasaki, K., J.-J. Yin, W. K. Subczynski, J. S. Hyde, and A. Kusumi. 2001. Pulse EPR detection of lipid exchange between protein-rich raft and bulk domains in the membrane: methodology development and its application to studies of influenza viral membrane. *Biophys. J*. 80: 738–748.

36. Wisniewska, A., and W. K. Subczynski. 2006. Accumulation of macular xanthophylls in unsaturated membrane domains. *Free Radic. Biol. Med*. 40:1820–1826.

37. Wisniewska, A., and W. K. Subczynski. 2006. Distribution of macular xanthophylls between domains in a model of photoreceptor outer segment membranes. *Free Radic. Biol. Med*. 41:1257–65.

38. Kusumi, A., W. K. Subczynski, and J. S. Hyde. 1982. Oxygen transport parameter in membranes as deduced by saturation recovery measurements of spin-lattice relaxation times of spin labels. *Proc. Natl. Acad. Sci. USA*. 79:1854–1858.

39. Subczynski, W. K., L. E. Hopwood, and J. S. Hyde. 1992. Is the mammalian cell plasma membrane a barrier to oxygen transport? *J. Gen. Physiol*. 100:69–87.

40. Subczynski, W. K., R. N. A. H. Lewis, R. N. McElhaney, R. S. Hodges, J. S. Hyde, and A. Kusumi. 1998. Molecular organization and dynamics of 1-palmitoyl-2-oleoylphosphatidylcholine bilayers containing a transmembrane α-helical peptide. *Biochemistry*. 37: 3156–3164.

41. Subczynski, W. K., M. Pasenkiewicz-Gierula, R. N. McElhaney, J. S. Hyde, and A. Kusumi. 2003. Molecular dynamics of 1-palmitoyl-2-oleoylphosphatidylcholine membranes containing transmembrane α-helical peptides with alternating leucine and alanine residues. *Biochemistry*. 42:3939–3948.

42. Shimshick, E. J., and H. M. McConnell. 1973. Lateral phase separation in phospholipid membranes. *Biochemistry*. 12:2351–2360.

43. Recktenwald, D. J., and H. M. McConnell. 1981. Phase equilibria in binary mixture of phosphatidylcholine and cholesterol. *Biochemistry*. 20:4505–4510.

44. Kusumi, A., W. K. Subczynski, M. Pasenkiewicz-Gierula, J. S. Hyde, and H. Merkle. 1986. Spin-label studies on phosphatidylcholine-cholesterol membranes: effects of alkyl chain length and unsaturation in the fluid phase. *Biochim. Biophys. Acta*. 854:307–317.

45. Almeida, P. F. F., W. L. C. Vaz, and T. E. Thompson. 1992. Lateral diffusion in the liquid phases of dimyristoyl/cholesterol bilayers: a free volume analysis. *Biochemistry*. 31:6739–6747.

46. Sanson, A., M. Ptak, J. L. Rignaud, and C. M. Gary-Bobo. 1976. *Chem. Phys. Lipids*. 17:435–444.

47. Egret-Charlier, M., A. Sanson, M. Ptak, and O. Bouloussa. 1978. Ionization of fatty acids at lipid-water interface. *FEBS Lett*. 89:313–316.

48. Kusumi, A., W. K. Subczynski, and J. S. Hyde. 1982. Effects of pH on ESR spectra of stearic acid spin labels in membranes: probing the membrane surface. *Fed. Proc*. 41:1394. (Abstr.)

49. Hyde, J. S., and W. K. Subczynski. 1989. Spin-label oximetry. *In* Biological magnetic resonance. Vol. 8. Spin labeling: theory and applications. L. J. Berliner and J. Reuben, editors. Plenum Press, New York. 399–425.

50. Subczynski, W. K., C. C. Felix, C. S. Klug, and J. S. Hyde. 2005. Concentration by centrifugation for gas exchange EPR oximetry measurements with loop-gap resonators. *J. Magn. Reson*. 176:244–248.

51. Yin, J. J., M. Pasenkiewicz-Gierula, and J. S. Hyde. 1987. Lateral diffusion of lipids in membranes by pulse saturation recovery electron spin resonance. *Proc. Natl. Acad. Sci. USA*. 84:964–968.

52. Hyde, J. S. 1998. Saturation recovery. *In* Foundations of modern EPR. G. R. Eaton, S. S. Eaton, and K. M. Salikhov, editors. World Scientific, Singapore. 607–618.

53. Chiang, Y.-W., J. Zhao, J. Wu, Y. Shimoyama, J. H. Freed, and G. W. Feigenson. 2005. New method for determining tie-lines in coexisting membrane phases using spin-label ESR. *Biochim. Biophys. Acta*. 1668:99–105.

54. Swamy, M. J., L. Klain, M. T. Ge, A. K. Smith, D. Holowka, B. Baird, and J. H. Freed. 2006. Coexisting domains in the plasma membranes of live cells characterized by spin-label ESR spectroscopy. *Biophys. J.* 90:4452–4465.

55. Windrem, D. A., and W. Z. Plachy. 1980. The diffusion-solubility of oxygen in lipid bilayers. *Biochim. Biophys. Acta.* 600:655–665.

56. Hyde, J. S., and W. K. Subczynski. 1984. Simulation of ESR spectra of the oxygen-sensitive spin-label probe CTPO. *J. Magn. Reson.* 56: 125–130.

57. Subczynski, W. K., and J. S. Hyde. 1984. Diffusion of oxygen in water and hydrocarbons using an electron spin resonance spin-label technique. *Biophys. J.* 45:743–748.

58. Fujiwara, T., K. Ritchie, H. Murakoshi, K. Jacobson, and A. Kusumi. 2002. Phospholipids undergo hop diffusion in compartmentalized cell membrane. *J. Cell Biol.* 157:1071–1081.

59. Loura, L. M. S., A. Fedorov, and M. Prieto. 2001. Fluid-fluid membrane microheterogenity: a fluorescence resonance energy transfer study. *Biophys. J.* 80:778–788.

60. Subczynski, W. K., and J. S. Hyde. 1981. The diffusion-concentration product of oxygen in lipid bilayers using the spin-label T1 method. *Biochim. Biophys. Acta.* 643:283–291.

61. Subczynski, W. K., and J. S. Hyde. 1983. Concentration of oxygen in lipid bilayer using a spin-label method. *Biophys. J.* 41:283–286.

62. Feigenson, G. W., and J. T. Buboltz. 2001. Ternary phase diagram of dipalmitoyl-PC/dilauroyl-PC/cholesterol: nanoscopic domain formation driven by cholesterol. *Biophys. J.* 80:2775–2788.

63. Heberle, F. A., J. F. Buboltz, D. Stringer, and G. W. Feigenson. 2005. Fluorescence methods to detect phase boundaries in lipid bilayer membranes. *Biochim. Biophys. Acta.* 1746:186–192.

64. Veatch, S. L., and S. L. Keller. 2003. Separation of liquid phases in giant vesicles of ternary mixtures of phospholipids and cholesterol. *Biophys. J.* 85:3074–3083.

65. Veatch, S. L., and S. L. Keller. 2003. A close look at the canonical ''raft mixture'' in model membranes. *Biophys. J.* 84:725–726.

66. Veatch, S. L., and S. L. Keller. 2005. Seeing spots: Complex phase behavior in simple membranes. *Biochim. Biophys. Acta.* 1746: 172–185.

67. Dietrich, C., L. A. Bagatolli, Z. N. Volovyk, N. L. Thompson, M. Levi, K. Jacobson, and E. Gratton. 2001. Lipid rafts reconstituted in model membranes. *Biophys. J.* 80:1417–1428.

68. Samsonov, A. V., I. Mihalyov, and F. S. Cohen. 2001. Characterization of cholesterol-sphingomyelin domains and their dynamics in bilayer membranes. *Biophys. J.* 81:1486–1500.

69. Samsonov, A. V., I. I. Mikhalyov, and F. S. Cohen. 2002. Detection of rafts in biological membranes. *Biophys. J.* 82:521a. (Abstr.)

70. McIntosh, T. J. 1978. The effect of cholesterol on the structure of phosphatidylcholine bilayers. *Biochim. Biophys. Acta.* 513:43–58.

71. Subczynski, W. K., A. Wisniewska, J.-J. Yin, J. S. Hyde, and A. Kusumi. 1994. Hydrophobic barriers of lipid bilayer membranes formed by reduction of water penetration by alkyl chain unsaturation and cholesterol. *Biochemistry.* 33:7670–7681.

72. Subczynski, W. K., and A. Kusumi. 1986. Effects of small amounts of cholesterol on gel-phase phosphatidylcholine membranes. *Biochim. Biophys. Acta.* 854:318–320.

73. Korlach, J., P. Schwille, W. W. Webb, and G. W. Feigenson. 1999. Characterization of lipid bilayer phases by confocal microscopy and fluorescence correlation spectroscopy. *Proc. Natl. Acad. Sci. USA.* 96:8461–8466.

74. Simons, K., and D. Toomre. 2000. Lipid rafts and signal transduction. *Nat. Rev. Mol. Cell Biol.* 1:1–39.

75. Gaffney, B. J., and D. Marsh. 1998. High-frequency, spin-label EPR of nonaxial lipid ordering and motion in cholesterol-containing membranes. *Proc. Natl. Acad. Sci. USA.* 95:12490–12493.

76. Ge, M., K. A. Field, R. Aneja, D. Holowka, B. Baird, and J. H. Freed. 1999. Electron spin resonance characterization of liquid ordered phase of detergent-resistant membranes from RBL-2H3 cells. *Biophys. J.* 77: 925–933.

77. Ge, M., A. Gidvani, H. A. Brown, D. Holowka, B. Baird, and J. H. Freed. 2003. Ordered and disordered phases coexist in plasma membrane vesicles of RBL-2H3 mast cells. *Biophys. J.* 85:1278–1288.

78. Veiga, M. P., J. L. R. Arrondo, F. M. Goni, A. Alonso, and D. Marsh. 2001. Interaction of cholesterol with sphingomyelin in mixed membranes containing phosphatidylcholine, studied by spin-label ESR and IR spectroscopies. A possible stabilization of gel-phase sphingolipid domains by cholesterol. *Biochemistry.* 40:2614–2622.

79. Wolf, C., and C. Chachaty. 2000. Compared effects of cholesterol and 7-dehydrocholesterol on sphingomyelin-glycerophospholipid bilayers studied by ESR. *Biophys. Chem.* 84:269–279.

80. Costa-Filho, A. J., Y. Shimoyama, and J. H. Freed. 2003. A2D-ELDOR study of the liquid ordered phase in multilamellar vesicle membranes. *Biophys. J.* 84:2619–2633.

81. Lou, Y., M. T. Ge, and J. R. Freed. 2001. A multifrequency ESR study of the complex dynamics of membranes. *J. Phys. Chem. B.* 105:11053–11056.

82. Kurad, D., G. Jeschke, and D. Marsh. 2004. Lateral ordering of lipid chains in cholesterol-containing membranes: high-field spin-label EPR. *Biophys. J.* 86:264–271.